Materials Research Bulletin 60 (2014) 868–871

Contents lists available at ScienceDirect

Materials Research Bulletin

journal homepage: www.elsevier.com/locate/matresbu

Free-standing anode of N-doped carbon nanofibers containing SnO_x for high-performance lithium batteries

Mingzhong Zou [a], Jiaxin Li [a,b], Weiwei Wen [a], Yingbin Lin [a], Heng Lai [a,*], Zhigao Huang [a,*]

[a] College of Physics and Energy, Fujian Normal University, Fuzhou 350007, China
[b] Fujian Institute of Research on the Structure of Matter, Chinese Academy of Sciences, Fuzhou 350002, China

ARTICLE INFO

Article history:
Received 26 February 2014
Received in revised form 16 September 2014
Accepted 28 September 2014
Available online xxx

Keywords:
A. Composite
B. Microstructure
D. Electrochemical properties
D. Energy storage

ABSTRACT

Free-standing paper of N-doped carbon nanofibers (NCNFs) containing SnO_x was prepared by electrospinning. The structure and morphology of the sample were analyzed by XRD, XPS, SEM, and TEM. The results show that nitrogen atoms were successfully doped into CNFs. The SnO_x were homogenously embedded in the N-doped CNFs *via* annealing treatment. Subsequently, the SnO_x NCNF paper was cut into disks and used as anodes for lithium ion batteries (LIBs). The anodes of SnO_x NCNFs exhibit excellent cycling stability and show high capacity of 520 mA h g^{-1} tested at a 200 mA g^{-1} after 100 cycles. More importantly, at a high current density of 500 mA g^{-1}, a large reversible capacity of 430 mA h g^{-1} after 100 cycles can still be obtained. The good electrochemical performance should be attributed to the good electronic conductivity from the NCNFs and the synergistic effects from NCNFs and SnO_x materials.

1. Introduction

Ultra-thin and flexible lithium batteries (LIBs) with high-energy and power density have risen as important devices for the increasing development of soft portable electronic equipment, such as roll-up displays and wearable devices [1–3]. Significant research effort has been devoted to find new anode materials and new electrode structure designs to improve energy densities for this kind of LIBs.

As an anode material in LIBs, graphite is commercially used but its theoretical capacity is only 372 mA h g^{-1}. Furthermore, the anode materials in commercial lithium batteries are usually coated on Cu foil to form electrodes. The Cu foil is a relatively heavy component in battery, which is comparable in weight to the anode active material. Such design makes these anode electrodes with low mass energy density not accessible for ultra-thin and flexible LIBs with high-energy and power density. A recently emerging solution is to use carbon nanofiber (CNF) paper to form free-standing electrodes for LIBs, not needing any binders and current collectors [4]. In addition, free-standing CNF electrodes have shown lightweight, good flexibility, and excellent mechanical strength, thereby improving the specific mass capacity and the cycling performance for LIBs. However, their low reversible capacities usually around 200–300 mA h g^{-1} hamper the practical use for LIBs [5]. To improve the effective capacity, a second phase of active material with higher capacity should be introduced into the CNF-based electrodes [6]. Tin-based materials as anodes have attracted extensive research because their high theoretical capacities of 994 and 782 mA h g^{-1} for metallic tin and tin dioxide (SnO_2), respectively, both more than two times the value of the conventional graphite anode [7,8]. More importantly, CNFs have been used as electronic conducting framework to improve the lithium storage properties of metal oxides including tin-based materials. In this regard, MnO_x/CNF [9], SnCo/CNF [10], and NiO/CNF [11] composites are proved to be able to improve electrochemical properties for LIBs. One thing to be noted is that N-doping process can generate extrinsic defects and form a disordered carbon structure, thus enhancing the Li^+ intercalation properties. Besides, N-doping can improve the reactivity and electric conductivity, and enhance the Li^+ storage kinetics [12,13]. Recently, several strategies including hydrothermal method [14,15], thermal CVD [16], annealing under N-containing atmosphere [17], and simple polymerization-pyrolysis [18,19] have been developed to obtain N-doping materials. Thus, to develop free-standing N-doped CNFs embedded with a second phase of active material as

* Corresponding authors. Tel.: +86 591 22867577; fax: +86 591 22867577.
E-mail addresses: ljx3012982@yahoo.com, ljx@fjirsm.ac.cn (J. Li), laiheng@fjnu.edu.cn (H. Lai), zghuang@fjnu.edu.cn (Z. Huang).

http://dx.doi.org/10.1016/j.materresbull.2014.09.086
0025-5408/

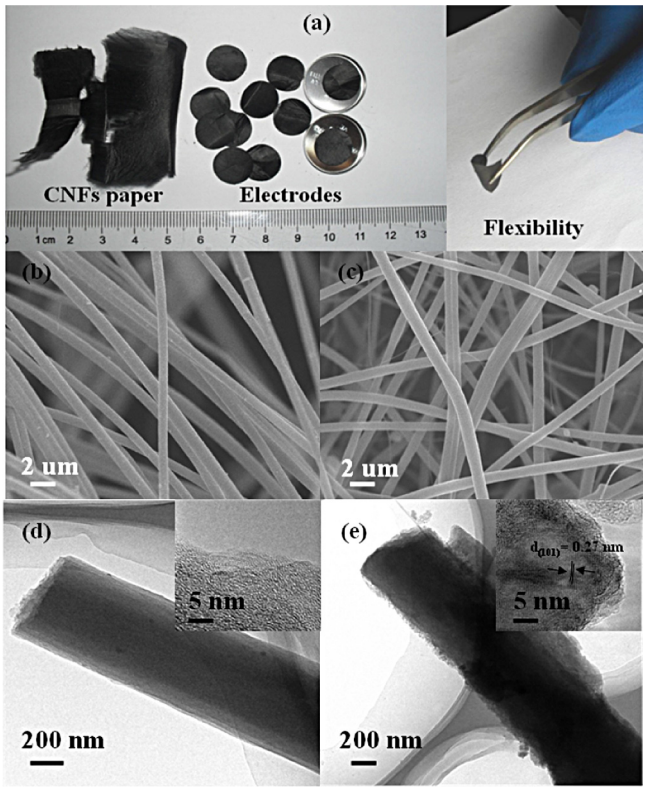

Fig. 1. (a), Digital camera images of CNF paper, CNF electrodes; (b) and (c), SEM images of the NCNFs and SnO_x NCNFs; (d) and (e), TEM and the corresponding HR-TEM images of the NCNFs and SnO_x NCNFs.

high-performance anodes for LIBs *via* a simple method is highly desired.

In this paper, free-standing papers of N-doped CNFs embedded with SnO_x particles have been prepared by electrospinning and directly used as anodes for LIBs. These free-standing anodes can afford good rate properties and excellent cycling stability with a high reversible capacity of ~430 mA h g^{-1} even after 100 cycles under a relatively high current density of 500 mA g^{-1}.

2. Experimental

2.1. Materials synthesis

All chemicals in experiment were of analytical grade and used as received. Typically, 2.0 g of polyacrylonitrile (PAN, M_w, 150,000) was dissolved in 20 ml of *N*,*N*-dimethylformamide (DMF), and then 2.0 g of $SnCl_2{\cdot}2H_2O$ was added to form a mixed solution. After vigorous stirring for 40 h at 60 °C, a sticky sol was obtained. For comparison, 20 ml of DMF solution containing 2.0 g PAN was also prepared without adding $SnCl_2{\cdot}2H_2O$. A 15 kV high voltage was used for electrospinning. The speed rate and distance were set up at 0.6 ml h^{-1} and 15 cm, respectively. The PAN nanofibers were collected on a rounded collector, and then dried for 24 h in vacuum at 80 °C. The dried nanofibers were further stabilized in air at 260 °C for 3 h with a heating rate of 2 °C min^{-1}. Finally, the stabilized nanofibers were annealed in a Ar flow at 830 °C for 1 h with a heating rate of 2 °C min^{-1} for forming N-doping CNFs (NCNFs). The self-standing NCNF paper was cut into disks (ϕ = 1.25 cm, wt = 1.5–2.0 mg), directly using as electrodes.

2.2. Materials characterization

These samples were characterized by X-ray diffraction (XRD, RIGAKU SCXmini), X-ray photoelectron spectroscopy (XPS, VG Scientific ESCALAB MK II), scanning electron microscope (SEM, JSM-6700F) and transmission electron microscope (TEM, Tecnai G2 F20).

2.3. Electrochemical measurements

The electrochemical behaviors were measured *via* CR2025 coin-type cells assembled in a dry argon-filled glove box. The cell consisted of NCNF anode and lithium sheet cathode which were separated by a Celgard 2300 membrane and electrolyte of 1 M $LiPF_6$ in EC:EMC:DMC (1:1:1 in volume). The cells were cycled by LAND2001A at room temperature. Cyclic voltammetry curves (CVs) were tested on a CHI660D Electrochemical Workstation.

3. Results and discussion

Fig. 1(a)–(e) shows digital camera images of CNF paper and CNF electrodes, SEM images of the NCNFs and SnO_x NCNFs, TEM and the corresponding HR-TEM images of the NCNFs, and SnO_x NCNFs, respectively. From Fig. 1(a), it is found that the free-standing electrodes have a good flexibility. From Fig. 1(b) and (c), one notices that both of the NCNFs and SnO_x NCNFs with the diameter ranging from 400 to 700 nm, are randomly oriented, continuous, and interconnected. Unlike the NCNFs (Fig. 1(d)) with a smooth surface, the SnO_x NCNFs observed in Fig. 1(e) reveals a rough morphology. The inset of HR-TEM image shown in Fig. 1(e) reveals the interplanar spacing of 0.27 nm, corresponding to the (1 0 1) plane of Sn alloy in SnO_x NCNFs.

The XRD pattern of the as-obtained SnO_x NCNFs is shown in Fig. 2(a). All the diffraction peaks were readily indexed to Sn [JCPDS Card No. 65-0296] and SnO_2 [JCPDS Card No. 33-1374]. No other impurities could be detected, except for an additional peak at ~26° taken from CNFs. The XPS for N1s spectra of the SnO_x NCNFs is shown in Fig. 2(b). Three fitted component peaks at 401.5, 400.1, and 398.3 eV are respectively assigned to quaternary, pyrrolic, and

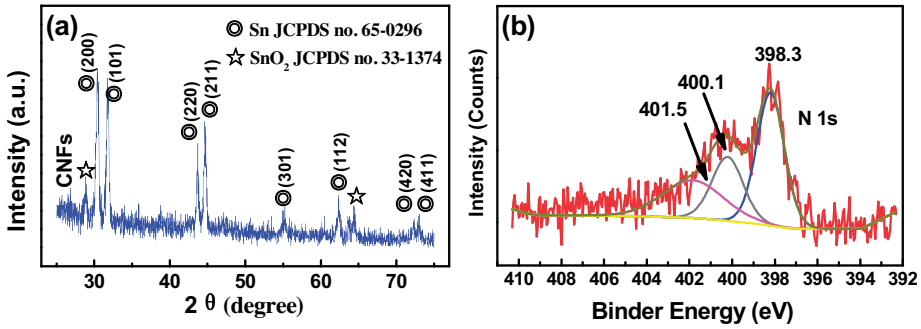

Fig. 2. (a), XRD pattern of the SnO_x NCNFs; (b), typical XPS spectra of N1s of the SnO_x NCNFs.

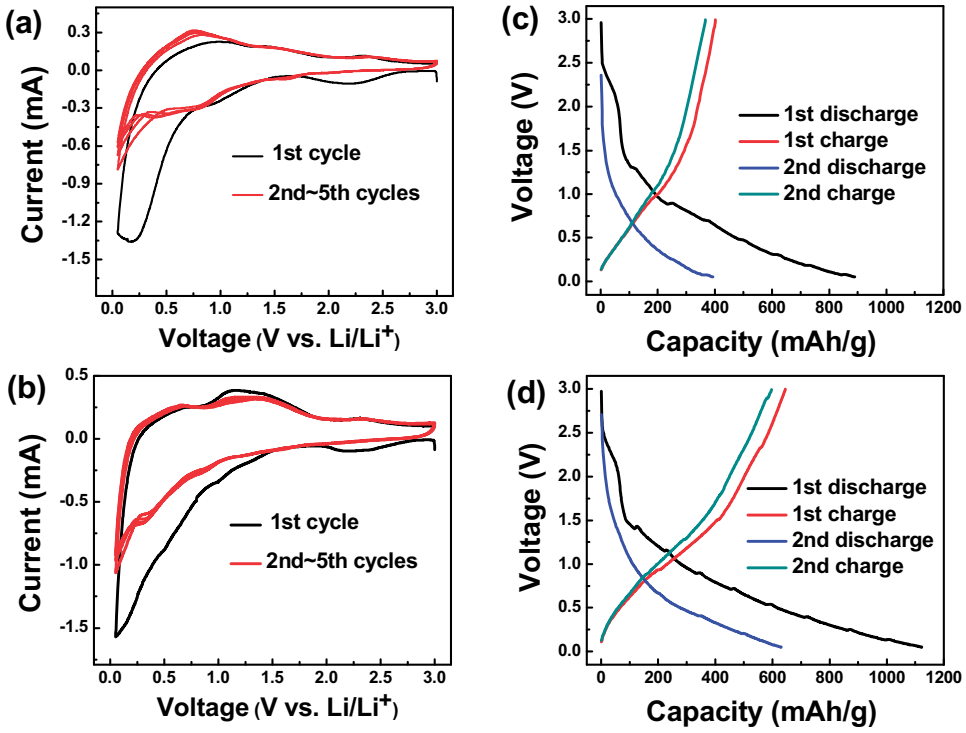

Fig. 3. Cyclic voltammetry curves and first two discharge–charge curves between 0.05 and 3 V of Li insertion/extraction into/from two electrodes: (a, c) NCNF electrodes and (b, d) SnO_x NCNF electrodes.

pyridinic nitrogen [20]. This result indicates that N was successfully doped into carbon nanofibers forming the NCNFs [13,20].

Fig. 3(a) and (b) shows the CVs of NCNF and SnO_x NCNF electrodes at the first 5 cycles at a scan rate of 0.5 mV s^{-1}, respectively. Fig. 3(a) shows that the shape of the 1st CVs for NCNF electrode is similar to other CNT-based electrodes [21]. All the redox peaks after the 1st CVs in NCNF electrode overlap well, indicating good electrochemical reversibility. Moreover, in the 1st cathodic scan in Fig. 3(b), the reduction peaks from 0.80 and 0.40 V related to the formation of a solid electrolyte interphase (SEI) layer (Eq. (1)) in SnO_x and the peak at around 0.70 V could also be assigned to the reduction of SnO_2 to Sn alloy and the formation of Li_2O (Eq. (2)). The peaks located around 0.05 and 0.30 V can be ascribed to the forming of Li_xSn (Eq. (3)) and lithium insertion in NCNFs. The oxidation peaks from 0.10 to 0.60 V correspond to lithium extraction from NCNFs, de-alloying of Li_xSn (Eq. (3)). Compared to the NCNFs (Fig. 3(a)), broad peaks appearing from 1.10 to 1.80 V in charged CVs correspond to the oxidation of Sn to SnO_2, implying that reaction of Eq. (2) is partially reversible in this case. Moreover, the well overlapped 2nd and 5th cycles are indicative of good capacity retention. Accordingly, the discharge/charge (D/C) profiles of the NCNF electrodes and SnO_x NCNF electrodes in the first two cycles at a current density of 200 mA g^{-1} are presented in Fig. 3(c) and (d). The voltage plateaus shown in D/

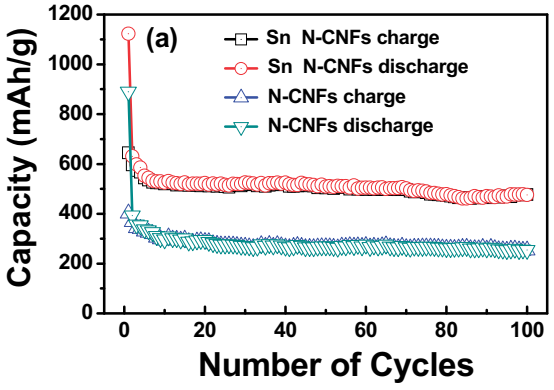

Fig. 4. Cycling performance of NCNF electrodes and SnO_x NCNF electrodes at a current density of 200 mA g^{-1}.

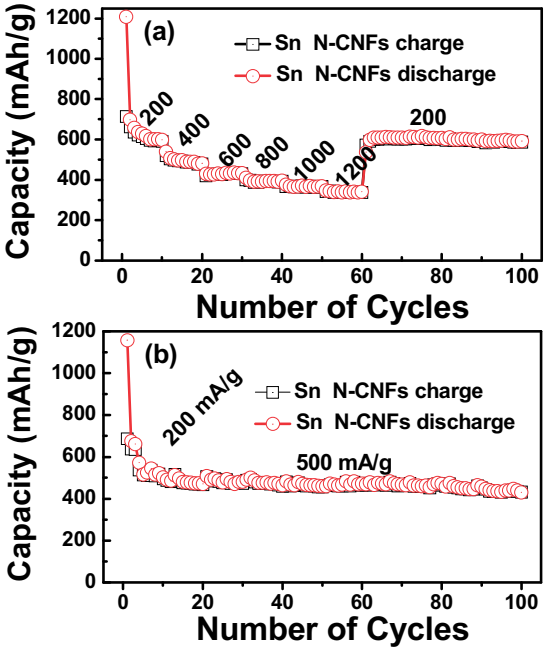

Fig. 5. Cycling performance of NCNF electrodes and SnO_x NCNF electrodes: (a) at various current rates and (b) at a large current density of 500 mA g^{-1}.

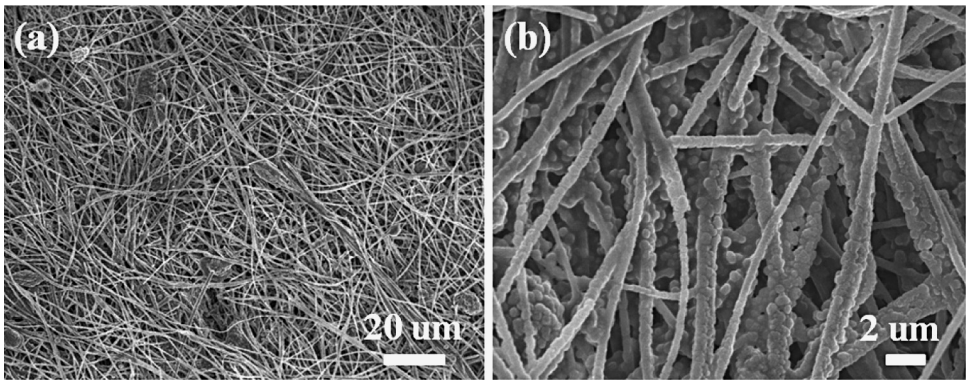

Fig. 6. SEM and the magnified SEM images of the SnO_x NCNFs after test.

C curves for the NCNF and SnO_x NCNF electrodes are consistent with the CV observation.

$$Li^+ + e^- + \text{electrolyte} \rightarrow \text{SEI (Li)} \quad (1)$$

$$SnO_2 + 4Li^+ + 4e^- \rightarrow Sn + 2Li_2O \quad (2)$$

$$Sn + xLi^+ + xe^- \leftrightarrow Li_xSn\ (0 \le x \le 4.4) \quad (3)$$

Fig. 4 compares the cycling performance of these two self-standing anodes at 200 mA g^{-1}. Apparently, the SnO_x NCNF electrode exhibits a significantly improved reversible capacity. After 100 cycles, the capacities for these two samples maintain stable with the increasing cycle number. In addition to good electrochemical stability, the rate performance of SnO_x NCNFs was also tested by changing the current density. Each fairly stable capacities at different current densities from 200 to 1200 mA g^{-1} can be observed in Fig. 5(a). When the current was reduced back to 200 mA g^{-1}, the SnO_x NCNFs can still deliver a reversible capacity of 570 mA h g^{-1}, implying the good rate stability. Moreover, the cycle performance of the SnO_x NCNF anode at a relatively high current densities of 500 mA g^{-1} after being activated at 200 mA g^{-1} in the first three cycles. As presented in Fig. 5(b), the reversible capacity can still stabilize at 430 mA h g^{-1} after 100 cycles, which is higher than the theoretical capacity of commercial graphite of 372 mA h g^{-1}.

The good performance obtained in self-standing SnO_x NCNF electrode could be mainly attributed to the synergistic effects of the contribution of NCNF supporter and the SnO_x materials. Fig. 6 shows SEM and the magnified SEM images of the SnO_x NCNFs after test. It is found from Fig. 6(a) that the SnO_x NCNFs are randomly oriented, continuous, and interconnected, being similar to the original sample. Fig. 6(b) shows that the fibrous morphology changes significantly due to the volume expansion of SnO_x during D/C process. There were no active materials falling off from the NCNFs. Moreover, there are still lots of macropores in the free-standing electrode, buffering the strains generated in the D/C process. Therefore, the cycling capability can be stabilized after long test. These results indicate that the electrode architecture has potential for use in high-energy and durable lithium ion batteries.

4. Conclusion

In summary, free-standing anodes of SnO_x NCNFs with good electrochemical performance have been fabricated *via* a facile electrospinning method. These anodes delivered a high reversible capacity of 520 mA h g^{-1} cycled at 200 mA g^{-1} after 100 cycles and a superior rate capability. Hereinto, NCNFs not only serve as conductive supporter, but also can effectively alleviate the expansion of SnO_x materials and prevent aggregation in the D/C process. In addition, the free-standing anode with the porous structure can efficiently facilitate faster Li^+ transfer and reduces polarization. Most of all, this facile approach is suitable for boosting the electrochemical properties of anode materials for LIBs.

Acknowledgement

We acknowledge the financial support by the Natural Science Foundations of China (No. 21203025, No. 51202031, No. 11004032, and No. 11074039).

References

[1] B. Liu, X. Wang, H. Chen, Z. Wang, D. Chen, Y.B. Cheng, C. Zhou, G. Shen, Sci. Rep. 3 (2013) 1622.
[2] L. Noerochim, J.-Z. Wang, S.-L. Chou, D. Wexler, H.-K. Liu, Carbon 50 (2012) 1289–1297.
[3] B. Wang, X. Li, B. Luo, Y. Jia, L. Zhi, Nanoscale 5 (2013) 1470–1474.
[4] B. Zhao, R. Cai, S. Jiang, Y. Sha, Z. Shao, Electrochim. Acta 85 (2012) 636–643.
[5] J.-Z. Wang, C. Zhong, S.-L. Chou, H.-K. Liu, Electrochem. Commun. 12 (2010) 1467–1470.
[6] J.-G. Wang, Y. Yang, Z.-H. Huang, F. Kang, Mater. Lett. 72 (2012) 18–21.
[7] J. Li, Y. Zhao, N. Wang, L. Guan, Chem. Commun. (Camb.) 47 (2011) 5238–5240.
[8] W. Yue, S. Yang, Y. Liu, X. Yang, Mater. Res. Bull. 48 (2013) 1575–1580.
[9] Z. Lin, L. Ji, M.D. Woodroof, X. Zhang, J. Power Sources 195 (2010) 5025–5031.
[10] B.-O. Jang, S.-H. Park, W.-J. Lee, J. Alloys and Compd 15 (2014) 325–330.
[11] B. Wang, J.L. Cheng, Y.P. Wu, D. Wang, D.N. He, Electrochem. Commun. 23 (2012) 5–8.
[12] P. Ayala, R. Arenal, M. Rümmeli, A. Rubio, T. Pichler, Carbon 48 (2010) 575–586.
[13] B.-H. Kim, K. Seung Yang, H.-G. Woo, Mater. Lett. 93 (2013) 190–193.
[14] X.B. Chen, Y.B. Lou, A.C. Samia, C. Burda, J.L. Gole, Adv. Funct. Mater. 15 (2005) 41–49.
[15] J. Zhang, J. Xi, Z. Ji, J. Mater. Chem. 22 (2012) 17700.
[16] H. Yue, F. Li, Z. Yang, J. Tang, X. Li, D. He, Mater. Lett. 120 (2014) 39–42.
[17] G. Zhang, J. Zhu, W. Zeng, S. Hou, F. Gong, F. Li, C.C. Li, H. Duan, Nano Energy 9 (2014) 61–70.
[18] X. Zhao, D. Xia, J. Yue, S. Liu, Electrochim. Acta 116 (2014) 292–299.
[19] J. Li, M. Zou, Y. Zhao, Z. Huang, L. Guan, RSC Adv. 3 (2013) 19251.
[20] B.P. Vinayan, S. Ramaprabhu, J. Mater. Chem. A 1 (2013) 3865.
[21] J.-X. Li, Y. Zhao, L.-H. Guan, Electrochem. Commun. 12 (2010) 592–595.